THERMAL EFFECTS ON STELLAR NEUTRON CAPTURE REACTIONS USING A QUANTUM DYNAMICAL MODEL*

N. Lightfoot, P. Stevenson, A. Diaz-Torres

Department of Physics, University of Surrey
Guildford GU2 7XH, Surrey, United Kingdom

Received 13 October 2025, accepted 12 January 2026, published online 31 March 2026

Neutron capture reactions in high-temperature environments play a vital role in our understanding of the age of the universe, as well as the function of nucleosynthesis in the creation of the heavy elements. In general, the temperatures characterising these reactions are variable and can be split into two separate processes: the slow (s) and rapid (r) neutron capture processes. In this work, thermal effects are introduced at the initialisation of the wave-packet with an implementation of the time-dependent coupled channels wave-packet (TDCCWP) method. The agreement of this method with the already accepted CCFULL method is explored for the $n + ^{186}$ Os reaction. Then, a comparison of thermally-dependent cross sections are made, where a decrease in the cross section is found for an increasing temperature, along with a decrease of 19% in the reaction rate when a temperature-dependent cross section is used.

DOI:10.5506/APhysPolBSupp.19.1-A7

1. Introduction

The reaction chain of osmium isotopes plays a central role in estimating the age of the universe through the Re–Os cosmic chronometer [1]. The abundance of ^{187}Os in the universe is created by two different pathways. The first is the β^- decay of ^{187}Re to ^{187}Os. This decay has a half-life of 42.3 Gyr [2] which is significantly longer than the estimated age of the universe of 15 ± 2 Gyr [3]. Therefore, the ratio between the total and amount of decayed ^{187}Re, making ^{187}Os, can give an estimate for the age of the universe. However, the second pathway, the $^{186}\mathrm{Os} + n$ reaction, also needs to be accounted for in the total abundance for ^{187}Os in order to estimate the age of the universe in network calculations.

* Presented at the XXXVIII Mazurian Lakes Conference on Physics, Piaski, Poland, August 31–September 6, 2025.

^{186}Os is also vital in exploring the creation of the neutron-rich nuclei in the universe. The isotopes $^{186-188}$Os are all dominated by the s-process neutron capture mechanism which acts at temperatures present in the stellar burning phase, around 50–200 million Kelvin (5–20 keV). This connection to temperatures has been used previously in the Hauser–Feshbach calculations, TALYS [4] and NON-SMOKER [5], where cross sections are weighted by Boltzmann factors to account for thermally populated excited states [6, 7]. However, in TDCCWP, the temperature dependence is introduced at the initialisation step of the wave-packet and then allowed to react [8, 9]. In general, thermal effects have been included in experimental results using theoretical models to generate the Stellar Enhancement Factor (SEF) to give a low-temperature experimental cross section a scaled result for astrophysical temperature ranges [1].

Previously, static coupled channels methods, CCFULL and FRESCO, that solve stationary coupled channels equations of motion have been used to extract transmission coefficients [10, 11]. In the TDCCWP method, a quantum dynamical model is used in order to incorporate the propagation of a thermalised wave-packet on a grid as it interacts with the target nucleus. Specifically, this work focuses on looking at the microscopic interactions when thermal effects are included from the beginning of the reaction.

In Section 2, the TDCCWP model will be highlighted through the previous $^{188}\mathrm{Os} + n$ case study, exploring how deformation changes the coupling potentials used. Section 3 will then compare the results of the $^{186}\mathrm{Os} + n$ reaction against previous models and describe the results of including thermal effects on cross sections and reaction rates. Lastly, in Section 4, the conclusions and next steps are explored.

2. Theoretical framework

Details of the TDCCWP model and a comparison to the previous Hauser–Feshbach style calculations used here can be found in Ref. [8], which highlights this method applied to the $^{188}\mathrm{Os} + n$ reaction as a test case. Here, the ^{186}Os isotope will be used due to its relevance in the Re–Os clock.

2.1. Exploring the dynamical model

In Fig. 1, the propagation of the ground-state wave-packet can be seen. The wave-packet is initialised at a radius $x_0 = 150$ fm and propagates using a Chebyshev representation of the exponential time-evolution operator [12]. This wave-packet represents the radial motion between the neutron projectile and osmium target. The internal nuclear potential is calculated from a Hartree–Fock many-body model [13]. At small radii, this potential reflects and absorbs a portion of the wave-packet. The final state is determined

when the expectation value of the radial position is larger than x_0 and the expectation value of the momentum is positive, otherwise it referrs to the wave-packet moving away from the target. Figure 1 shows the single-channel case, where the coupled channels model allows for the inclusion of several excitations of the target [10]. Each energy level has its own component of the wave-packet that moves along the grid and interacts with the nuclear and coupling potentials of the system [14–16].

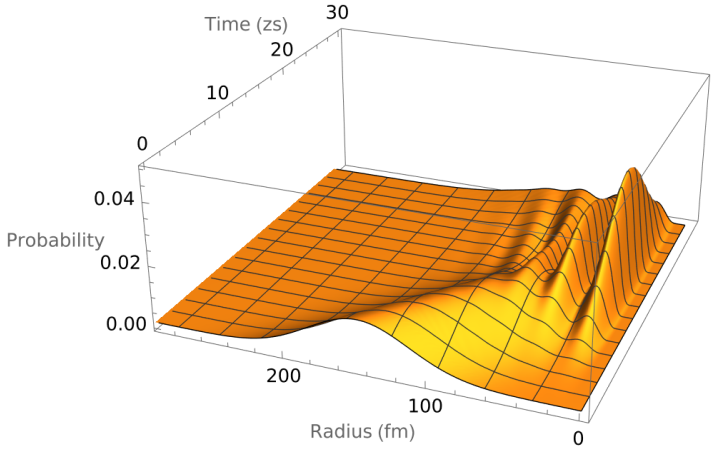

Fig. 1. Dynamical propagation of the wave-packet, corresponding to the interaction of a neutron with the ^{186}Os target. Initially, the wave-packet has a radius, $x_0 = 150$ fm, and a spatial width, $\sigma_0 = 50$ fm. The calculation is complete once the average position of the recoiled wave-packet is x_0.

The remaining explanation of the propagation is presented in Ref. [8] for the ^{188}Os$+n$ test case and is grounded in the work done for fusion reactions in Refs. [9, 17–19]. A discussion of the importance of the deformation in the shape of the coupling potentials is shown in the next section.

2.2. Deformation changing coupling potentials

The monopole nuclear potential of the system accounts for the spherical shape of the target, whereas the quadrupole and hexadecapole deformation in the coupled channels scheme give the non-spherical shape of the nucleus and defines the coupling potentials. The solid lines in Fig. 2 show that a change in the β_2 deformation results in a change in the strength of the coupling potential, where a larger deformation corresponds to a stronger coupling potential. However, the dashed lines in Fig. 2 show that when the

β_4 deformation decreases, there is an increase in the depth and a decrease in the radius of the coupling potential. The deformation parameters used for the $^{186}\mathrm{Os} + n$ implementation are: $\beta_2 = 0.202$ and $\beta_4 = -0.059$ [20].

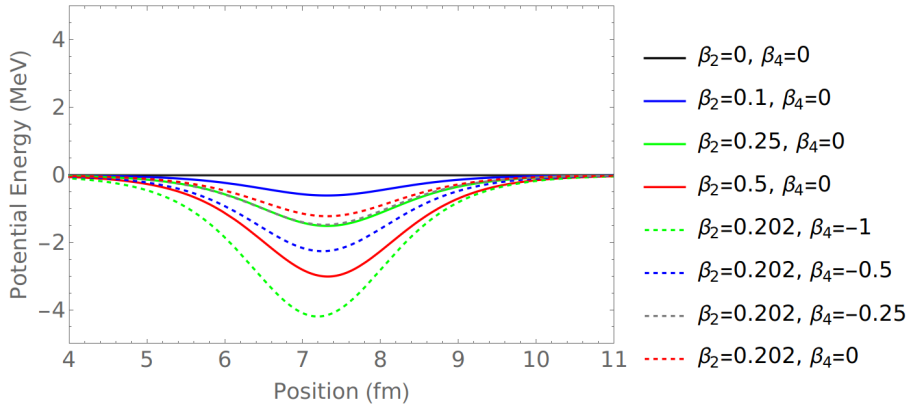

Fig. 2. The ground state to first excited state coupling potential is shown for variable quadrupole, β_2, deformation by the solid lines. The depth of the coupling potential increases with an increase in quadrupole deformation. The dashed lines show variable hexadecapole deformation with constant β_2. The coupling depth increases with decreasing β_4, while the radius decreases.

2.3. Calculating reaction rates

In typical reaction rate calculations, cross sections are weighted with Boltzmann factors to incorporate thermal effects at the cross-sectional level. However, in this TDCCWP model, the initialisation of the wave-packet includes a thermalisation step and then carries those thermal effects throughout the calculation. The reaction rate in terms of the new thermal dependence of the cross section is calculated as follows [21]:

$$\langle \sigma\, v \rangle = \sqrt{\frac{8}{\pi\mu}} \left(\frac{1}{kT}\right)^{\frac{3}{2}} \frac{\int_{E_i}^{E_f} \sigma(E,T)\, E\, P(E,T) \mathrm{d}E}{\int_{E_i}^{E_f} E\, P(E,T) \mathrm{d}E}\,. \tag{1}$$

This inclusion of temperature from the beginning of the calculation is done by using Boltzmann factors to prepare an initially thermalised wave-packet [8]. In the next section, the results of this temperature dependence are shown against previous models.

3. Results from ^{186}Os

3.1. Transmission coefficients and comparison against CCFULL

The CCFULL calculation is a static method that directly solves the coupled channels equations of motion at the end of the reaction to extract transmission coefficients directly [22]. The TDCCWP method gives the dynamical calculation of the $^{186}\mathrm{Os} + n$ reaction to describe the same transmission coefficients. In order to check the validity of the calculation, a comparison of the s-wave component of the two calculations are shown in Fig. 3. In general, CCFULL gives a larger capture probability than the TDCCWP calculation, however the two calculations are accurate within error to one another and show a similar shape against incident energies.

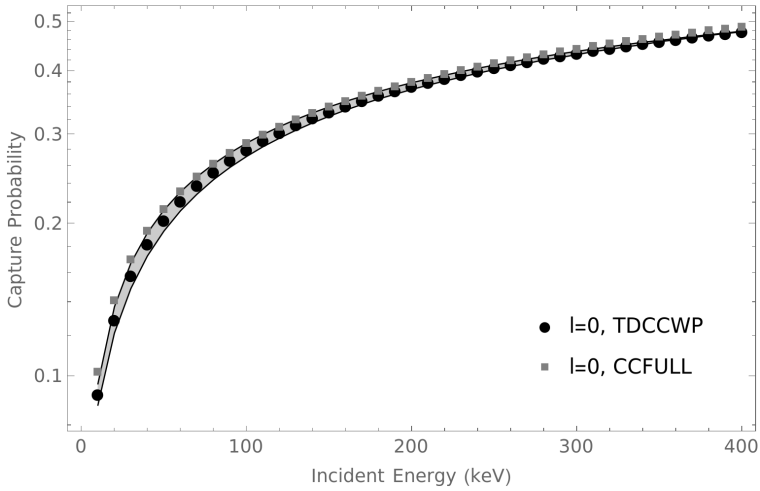

Fig. 3. Capture probabilities for the TDCCWP and CCFULL models for an s-neutron. The shaded region gives the error based on the difference in spatial widths, 50 to 80 fm, of the initial wave-packet which determines the error of the TDCCWP calculation [8].

3.2. Neutron capture cross sections

With the inclusion of thermal effects in the initialisation step of the wave-packet implementation [8], a reduction in cross section can be seen in Fig. 4 with an increase in temperature. The kink in the high-temperature cross section is due to the introduction of the kinematically closed state. This refers to the region of incident energies that is below the first excited state, 137.15 keV for ^{186}Os. In this region, only virtual excitations can occur, meaning that the portion of the wave-packet corresponding to the

excited state is stationary within the nuclear potential. Above this region, the wave-packet is allowed to propagate with a wave-number determined by $k_0 = \sqrt{\frac{2\mu(E_0-\epsilon)}{\hbar^2} - \frac{1}{2\sigma_0^2}}$, where ϵ is the excited state energy.

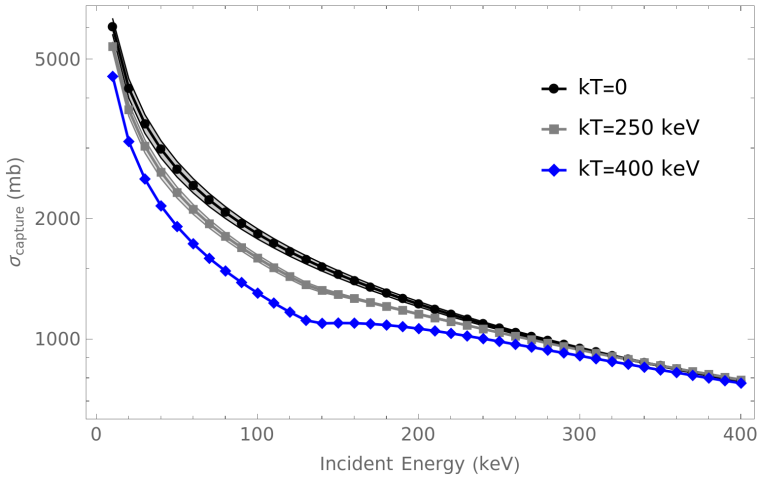

Fig. 4. Temperature-dependent capture cross sections for a $l = 0$ neutron on the ^{186}Os target as a function of the neutron incident energy in the range of 10–500 keV for three different thermal energies. The shaded regions highlight errors associated with the energy variance of the neutron energy.

Along with this transition between two regions in energy, also shown in Fig. 4 at the first excited state, there is a decrease in error when there is an increase in either the incident energy or the temperature. This error is calculated based on using a larger spatial width of the initial wave-packet which gives a smaller energy resolution [8]. Therefore, this increase in temperature and energy increases the computational accuracy of the model.

3.3. Reaction rates and the s-process

The neutron-rich osmium isotopes are predominantly created through the slow-neutron capture process. This process acts in temperature ranges of around 5–20 keV in thermal energy. Figure 5 shows the agreement of reaction rates between a temperature-dependent and -independent cross section inputted in the reaction rate for temperatures smaller than the first excited state. For the highest temperature, 500 keV, there is a decrease of 19%, with model error of the same order, as seen in the inset in Fig. 5 when a temperature-dependent cross section is used. This is due to higher temperatures resulting in a higher population in the first excited state and a higher speed of the neutron in the absorption region, which results in a higher prob-

ability of escaping capture. Furthermore, this reduces the capture probability as shown in Figs. 4 and 5. This could also suggest why these isotopes are dominated by the s-process reactions at lower temperatures rather than by processes at higher temperatures. However, these thermal energies are used to show the extent of the use of this model, since thermal energies this high are far above the actual temperatures present in s-process reactions which dominate for the $^{186-188}$Os isotopes.

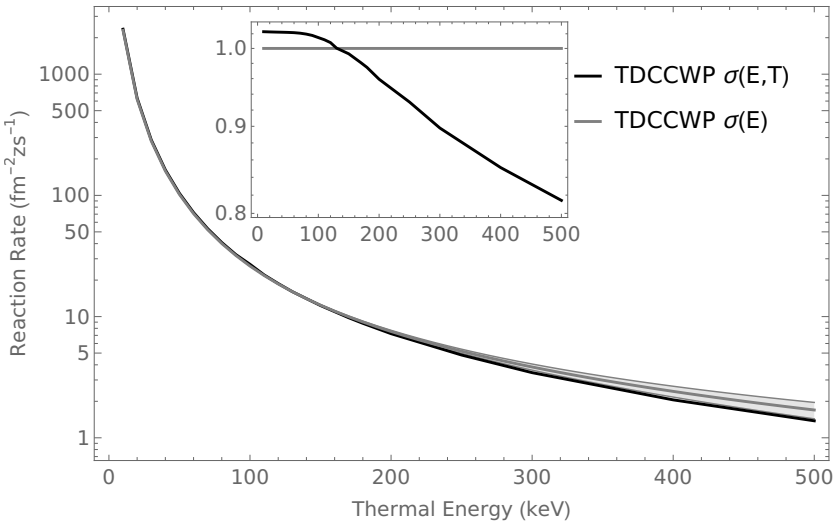

Fig. 5. Reaction rate calculated with (black line) and without (gray line) a temperature-dependent cross section. The reaction rate decreases when a temperature-dependent cross section is included in the reaction rate at temperatures beyond the first excited state. The band around the gray line shows the error against the same calculation using a wider wave-packet, 50 to 80 fm. The model error is of the same order as the changes between the two models. An inset graph shows the fraction between cross sections, $\frac{\sigma(E,T)}{\sigma(E)}$.

4. Conclusion

This paper outlines the results found using the TDCCWP method for the ^{186}Os$+n$ capture reaction. The results of this model were first validated using CCFULL, followed by highlighting the decrease in cross section with increasing temperature as well as a 19% reduction in the reaction rate for a thermal energy of 500 keV. Future work includes looking at the surrounding nuclei in the Re–Os reaction chain as well as applying the same model to other isotopes in other astrophysically significant regions.

This work was supported by the UK Science and Technology Facilities Council (STFC) under grants No. ST/Y509619/1, ST/V001108/1, and ST/Y000358/1.

REFERENCES

[1] M. Mosconi *et al.*, *Phys. Rev. C* **82**, 015803 (2010).
[2] M. Segawa *et al.*, *Phys. Rev. C* **76**, 022802 (2007).
[3] L. Kazakov *et al.*, «The Re Os clock revisited», proposal CERN-INTC-2000-040; INTC-P-125, 2000.
[4] A. Koning, S. Hilaire, S. Goriely, *Eur. Phys. J. A* **59**, 146 (2023).
[5] T. Rauscher, F.K. Thielemann, *At. Data Nucl. Data Tables* **75**, 1 (2000).
[6] F.K. Thielemann, T. Rauscher, «Nuclear Reactions in Evolving Stars (and Their Theoretical Prediction)» in: I. Tanihata, H. Toki, T. Kajino (Eds.) «Handbook of Nuclear Physics», *Springer*, Singapore 2023, pp. 3435–3490.
[7] T. Rauscher, *Int. J. Mod. Phys. E* **20**, 1071 (2011).
[8] N. Lightfoot, A. Diaz-Torres, P. Stevenson, arXiv:2509.12404 [nucl-th].
[9] G. Close, P. Stevenson, A. Diaz-Torres, *Phys. Lett. B* **870**, 139881 (2025).
[10] K. Hagino, N. Rowley, A.T. Kruppa, *Comput. Phys. Commun.* **123**, 143 (1999).
[11] C. Bustreo *et al.*, *Fusion Eng. Des.* **88**, 3141 (2013).
[12] R. Chen, H. Guo, *Comput. Phys. Commun.* **119**, 19 (1999).
[13] T.H.R. Skyrme, *Nucl. Phys.* **9**, 615 (1958).
[14] T. Vockerodt, A. Diaz-Torres, *Phys. Rev. C* **100**, 034606 (2019).
[15] T. Vockerodt, Ph.D. Thesis, University of Surrey, 2021.
[16] T. Vockerodt, A. Diaz-Torres, *Phys. Rev. C* **104**, 064601 (2021).
[17] I. Lee, A. Diaz-Torres, *Phys. Lett. B* **827**, 136970 (2022).
[18] I. Lee, Ph.D. Thesis, University of Surrey, 2023.
[19] I. Lee *et al.*, *Phys. Rev. C* **107**, 054609 (2023).
[20] T.F. Barker *et al.*, *Nucl. Phys. A* **258**, 43 (1976).
[21] B.R. Martin, «Nuclear and Particle Physics. An Introduction», *John Wiley & Sons Ltd*, 2006.
[22] K. Hagino, J.M. Yao, *Phys. Rev. C* **91**, 064606 (2015).